Iranian Journal of Science and Technology, Transactions of Mechanical Engineering (2022) 46:253–273
https://doi.org/10.1007/s40997-020-00421-1

RESEARCH PAPER

Metaheuristic Optimization of Rotating Multilayer Composite Tubes Under Internal Heating and Pressure

Saeid Kazemzadeh Azad[1] · **Tolga Akış**[1]

Received: 9 June 2020 / Accepted: 29 December 2020 / Published online: 21 January 2021

Abstract
Although analysis/design of multilayer assemblies has been always an active field of research, works on the optimal design of rotating multilayer composite tubes are very limited. This paper addresses the design optimization of rotating multilayer composite tubes under internal heating and pressure. For determining the structural responses, analytical solutions are provided based on different boundary conditions. The automated selection of optimal material as well as thickness optimization of pressurized multilayer assemblies is carried out under different angular speed and internal heating conditions using a metaheuristic algorithm. The corresponding optimum design for each angular speed as well as internal heating condition is sought, and the numerical results are discussed. The study provides general guidelines for conceptual design of rotating multilayer composite tubes subjected to internal heating and pressure.

Keywords Multilayer composite tubes · Discrete optimization · Optimal design · Evolutionary algorithms · Metaheuristics · von Mises yield criterion

1 Introduction

Optimization has long been recognized as an efficient process for improving the desirable properties of structural and mechanical engineering systems. Among the numerous optimization objectives, reducing the total design cost/weight is one of the common primary goals in practical engineering applications. For optimization of multilayer composite tubes, in general, the main goal is to achieve a minimum weight or cost-efficient assembly, which satisfies the prespecified design constraints (Sharifi et al. 2014; Apatay and Mack 2015). For this purpose, the optimum arrangement of material layers as well as the optimal thickness of each layer should be sought using a suitable design optimization algorithm. Indeed, structural response computations of multilayer composite tubes should also be accomplished as a part of the design process.

✉ Saeid Kazemzadeh Azad
saeid.azad@atilim.edu.tr; s.kazemzadeh.azad@gmail.com

Tolga Akış
tolga.akis@atilim.edu.tr

[1] Department of Civil Engineering, Atilim University, Ankara, Turkey

Many recent studies have focused on the analysis and design of multilayer composite assemblies under various loading, interface, and boundary conditions. Ootao et al. (1991), Lee et al. (2001), and Eraslan et al. (2003) investigated the thermal stresses in composite tubes under different thermal loading conditions. The studies performed by Tutuncu (1995) and Tzeng (2002) were based on the investigation of the stress response of rotating composite tubes. Akış and Eraslan (2005) investigated the yielding behavior of pressurized two-layer tightly fitted concentric tubes based on von Mises yield criterion. They in particular addressed the yielding of pressurized two-layer shrink-fitted composite tubes in Eraslan and Akis (2005). Moreover, Jahed et al. (2006) tackled the design optimization problem of multilayer cylinders for maximum fatigue life expectancy under the combined effects of autofrettage and shrink fit. Considering Tresca criterion, Sharifi et al. (2012) developed an analytical method for optimal design of shrink-fitted multilayer compound cylinders. The authors deduced that in the case of larger ratios of outer to inner radii, increasing the number of layers becomes more advantageous. Later, Sharifi et al. (2014) proposed an analytical method for optimum design of multilayer cylinders with respect to different objective functions including weight and cost. Miraje and Patil (2012) studied the thickness optimization of three-layer shrink-fitted

compound cylinders. Zhou et al. (2012) addressed the stress analysis as well as optimal design of a three-layer composite tube subjected to thermomechanical loads. In a closely related study, Apatay and Mack (2015) studied the optimization of rotating two-layered hollow cylinder subjected to internal heating or internal pressure. Recently, the effect of shrink-fitting on the optimum design of multilayer composite tubes has been studied in Kazemzadeh Azad and Akış (2019). The design optimization results obtained for multilayer composite tubes indicated that more economical solutions could be found if shrink-fitting parameters are considered as additional design variables. Although numerous studies have been conducted on the analysis/design of multilayer assemblies, limited work has been conducted so far on the design optimization of rotating multilayer composite tubes (Apatay and Mack 2015). Accordingly, the present paper is devoted to the design optimization of rotating multilayer composite tubes under internal heating and pressure.

Typically, the first step in an optimization process is to select a suitable algorithm considering the nature of solution variables, objective function, and problem constraints. It is generally known that conventional structural optimization methods, i.e., mathematical programming (Erbatur and Al-Hussainy 1992) and optimality criteria (Tabak and Wright 1981; Saka 1991) have been originally proposed for handling continuous optimization problems and basically depend on gradient information of objective functions. Accordingly, it is generally conceived that the aforementioned classical techniques are not suitable for handling discrete or non-differentiable problems. In the past few decades, many researchers employed non-traditional stochastic search algorithms, i.e., metaheuristics as alternative tools to the conventional optimization methodologies. Generally, metaheuristic approaches, such as genetic algorithms (Goldberg and Samtani 1986), particle swarm optimization (Kennedy and Eberhart 1995), ant colony optimization (Colorni et al. 1991), harmony search algorithm (Lee and Geem 2004), big bang-big crunch algorithm (Erol and Eksin 2006), etc., follow non-deterministic search strategies to locate the optimum or a reasonably near-optimum solution. The advantageous attributes of metaheuristic or evolutionary algorithms can be outlined as: global search features, derivative-free characteristics, ease of implementation, and capability of dealing with both discrete, continuous, or mixed-integer optimization problems. Considering the discrete nature of the design variables associated with the optimal design of rotating multilayer composite tubes, metaheuristic search techniques could be efficiently employed for handling such combinatorial optimization problems.

This paper investigates the weight and cost minimization of rotating multilayer composite tubes under internal heating and pressure based on von Mises yield criterion. In order to calculate the structural responses, analytical solutions are presented based on two different tube end conditions, namely generalized plane strain case (free ends), which assumes a uniform extension in the axial direction, and plane strain case (fixed ends) in which axial displacement is prevented. The optimum material selection and thickness optimization of one-, two-, and three-layer assemblies are carried out under different angular speed and internal heating conditions using a metaheuristic optimization algorithm. The optimum designs associated with different values of angular speed as well as internal heating are sought, and the obtained results are discussed. The numerical experiments, performed under different loading and tube end conditions, provide some general guidelines for preliminary or conceptual design of rotating multilayer composite tubes.

The present work is organized as follows: In the second section, the analytical solutions of rotating multilayer composite tubes under internal heating and pressure are described. The formulation of the optimization problem is stated in the third section. The fourth section briefly outlines the utilized metaheuristic algorithm. The numerical instances as well as the obtained results are given in the fifth section. Finally, the concluding remarks are summarized in the last section.

2 Analysis of Rotating Multilayer Assemblies

In this section, the analytical solutions developed to estimate the response of rotating one-, two-, and three-layer thick-walled tubes subjected to elevated temperature and pressure at the inner surface are presented. Here, cylindrical polar coordinates (r, θ, z) are employed and small deformations are presumed in the derivations. In addition, the multilayer assemblies are assumed to be tightly fitted and perfectly bonded. In derivations, the generalized plane strain solution is obtained first and reduced to plane strain state by equating the axial strain to zero.

2.1 Temperature Distribution

The assemblies are subjected to an elevated temperature of the inner surface and assumed to be in steady state. The temperature distribution for a long single-layer tube is governed by the following equation (Noda et al. 2003):

$$\frac{\mathrm{d}^2T}{\mathrm{d}r^2} + \frac{1}{r}\frac{\mathrm{d}T}{\mathrm{d}r} = 0 \tag{1}$$

where r is the radial coordinate and T is the temperature distribution (i.e., difference of absolute and reference temperature). The general solution is

$$T(r) = A \ln r + B \tag{2}$$

where A and B are the integration constants calculated based on the following boundary conditions:

$$T(a) = T_0 \text{ and } T(b) = 0 \tag{3}$$

Here, a and b are the inner and outer surface radii of the tube (see Fig. 1), respectively, and T_0 is the constant inner surface temperature. The temperature of the outer surface is assumed to be zero. Application of the boundary conditions gives

$$A = \frac{T_0}{\ln(a/b)} \text{ and } B = -\frac{T_0 \ln b}{\ln(a/b)} \tag{4}$$

For the two-layer assemblies, the same temperature distribution obtained for a single-layer tube in Eq. (2) is valid for both inner and outer layers and can be written as

$$T_1(r) = A_1 \ln r + B_1, \quad T_2(r) = A_2 \ln r + B_2 \tag{5}$$

where T_1 and T_2 are the temperature distributions in the inner ($a \le r \le r_1$) and outer ($r_1 \le r \le b$) layers, respectively. The following boundary conditions are valid for the two-layer tubes:

$$T_1(a) = T_0 \text{ and } T_2(b) = 0 \tag{6}$$

In addition, at the interface radius ($r = r_1$), both the temperatures and heat fluxes are equal, which gives

$$T_1(r_1) = T_2(r_1) \text{ and } k_1 \frac{\mathrm{d}T_1(r)}{\mathrm{d}r}\bigg|_{r=r_1} = k_2 \frac{\mathrm{d}T_2(r)}{\mathrm{d}r}\bigg|_{r=r_1} \tag{7}$$

where k_1 and k_2 denote the thermal conductivity of the inner and outer layers, respectively. Using these conditions, the integration constants are determined as

$$A_1 = \frac{k_2 T_0}{k_1 \ln(r_1/b) + k_2 \ln(a/r_1)} \tag{8}$$

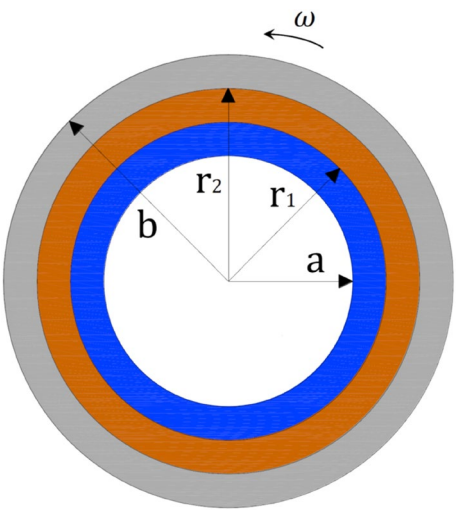

Fig. 1 Typical cross section of rotating multilayer composite tube

$$B_1 = T_0 - \frac{k_2 T_0 \ln a}{k_1 \ln(r_1/b) + k_2 \ln(a/r_1)} \tag{9}$$

$$A_2 = \frac{k_1 T_0}{k_1 \ln(r_1/b) + k_2 \ln(a/r_1)} \tag{10}$$

$$B_2 = -\frac{k_1 T_0 \ln b}{k_1 \ln(r_1/b) + k_2 \ln(a/r_1)} \tag{11}$$

Akin to the two-layer composite tubes, for the three-layer tubes, the temperature distributions in the inner ($a \le r \le r_1$), middle ($r_1 \le r \le r_2$) and outer ($r_2 \le r \le b$) layers can be stated as

$$T_1(r) = A_1 \ln r + B_1,\ T_2(r) = A_2 \ln r + B_2 \text{ and } T_3(r) = A_3 \ln r + B_3 \tag{12}$$

The boundary conditions are

$$T_1(a) = T_0 \text{ and } T_3(b) = 0 \tag{13}$$

and the interface conditions at the two interface radii (at $r = r_1$ and $r = r_2$) can be written as

$$T_1(r_1) = T_2(r_1), \quad T_2(r_2) = T_3(r_2) \tag{14}$$

$$k_1 \frac{\mathrm{d}T_1(r)}{\mathrm{d}r}\bigg|_{r=r_1} = k_2 \frac{\mathrm{d}T_2(r)}{\mathrm{d}r}\bigg|_{r=r_1}, \quad k_2 \frac{dT_2(r)}{dr}\bigg|_{r=r_2} = k_3 \frac{dT_3(r)}{dr}\bigg|_{r=r_2} \tag{15}$$

where k_1, k_2 and k_3 are the thermal conductivity of the inner, middle and outer layers, respectively. Application of these conditions yields

$$A_1 = \frac{k_2 k_3 T_0}{k_2 k_3 \ln(a/r_1) + k_1 k_3 \ln(r_1/r_2) + k_1 k_2 \ln(r_2/b)} \tag{16}$$

$$B_1 = T_0 - \frac{k_2 k_3 T_0 \ln a}{k_2 k_3 \ln(a/r_1) + k_1 k_3 \ln(r_1/r_2) + k_1 k_2 \ln(r_2/b)} \tag{17}$$

$$A_2 = \frac{k_1 k_3 T_0}{k_2 k_3 \ln(a/r_1) + k_1 k_3 \ln(r_1/r_2) + k_1 k_2 \ln(r_2/b)} \tag{18}$$

$$B_2 = \frac{k_1 T_0 \left[k_2 \ln(r_2/b) - k_3 \ln r_2\right]}{k_2 k_3 \ln(a/r_1) + k_1 k_3 \ln(r_1/r_2) + k_1 k_2 \ln(r_2/b)} \tag{19}$$

$$A_3 = \frac{k_1 k_2 T_0}{k_2 k_3 \ln(a/r_1) + k_1 k_3 \ln(r_1/r_2) + k_1 k_2 \ln(r_2/b)} \tag{20}$$

$$B_3 = -\frac{k_1 k_2 T_0 \ln b}{k_2 k_3 \ln(a/r_1) + k_1 k_3 \ln(r_1/r_2) + k_1 k_2 \ln(r_2/b)} \tag{21}$$

2.2 Elastic Solution

2.2.1 Generalized Plane Strain Case (Free Ends)

For a single-layer tube, using the common notation for the stresses and strains (Timoshenko and Goodier 1970), the generalized Hooke's law reads

$$\varepsilon_r = \frac{1}{E}\left[\sigma_r - \nu(\sigma_\theta + \sigma_z)\right] + \alpha T \tag{22}$$

$$\varepsilon_\theta = \frac{1}{E}\left[\sigma_\theta - \nu(\sigma_r + \sigma_z)\right] + \alpha T \tag{23}$$

$$\varepsilon_z = \frac{1}{E}\left[\sigma_z - \nu(\sigma_r + \sigma_\theta)\right] + \alpha T \tag{24}$$

Here, ε_i are the strain components, E the modulus of elasticity, ν the Poisson's ratio, α the coefficient of thermal expansion, σ_i the stress components in radial, circumferential, and axial directions, and T the temperature difference between the absolute and the reference temperatures. The strain–displacement relations ($\varepsilon_r = \mathrm{d}u/\mathrm{d}r$ and $\varepsilon_\theta = u/r$), and the equation of equilibrium in the radial direction

$$\frac{\mathrm{d}\sigma_r}{\mathrm{d}r} + \frac{\sigma_r - \sigma_\theta}{r} = -\rho\omega^2 r \tag{25}$$

form the basic elastic equations together with Eqs. (22) to (24). In Eq. (25) ρ and ω are the material density and angular speed, respectively. In case of generalized plane strain ($\varepsilon_z = \varepsilon_0 = \text{constant}$), the axial stress becomes

$$\sigma_z = E\varepsilon_0 + \nu(\sigma_r + \sigma_\theta) - E\alpha T \tag{26}$$

Combining the equations of the generalized Hooke's law with the strain displacement relations, substituting the axial stress into radial and circumferential stress expressions, and putting these two stress expressions into the equation of equilibrium (25), the governing differential equation for the single-layer tube can be obtained as

$$r^2\frac{\mathrm{d}^2u}{\mathrm{d}r^2} + r\frac{\mathrm{d}u}{\mathrm{d}r} - u = -\frac{(1+\nu)(1-2\nu)}{E(1-\nu)}\rho\omega^2 r^3 + \frac{(1+\nu)}{(1-\nu)}\alpha r^2\frac{\mathrm{d}T}{\mathrm{d}r} \tag{27}$$

The solution of the foregoing equation gives the radial displacement in a single-layer elastic tube. Here, the general solution can be stated as

$$u(r) = \frac{C_1}{r} + C_2 r - \frac{\rho\omega^2 r^3(1+\nu)(1-2\nu)}{8E(1-\nu)} + \frac{\alpha(1+\nu)}{r(1-\nu)}\int_a^r \lambda T(\lambda)\mathrm{d}\lambda \tag{28}$$

where C_1 and C_2 are arbitrary integration constants. The stresses in radial and circumferential directions are then computed as

$$\sigma_r = \frac{E}{(1+\nu)(1-2\nu)}\left[-\frac{C_1(1-2\nu)}{r^2} + C_2 + \varepsilon_0\nu\right] - \frac{r^2\omega^2(3-2\nu)\rho}{8(1-\nu)} - \frac{E\alpha}{r^2(1-\nu)}\int_a^r \lambda T(\lambda)\mathrm{d}\lambda \tag{29}$$

$$\sigma_\theta = \frac{E}{(1+\nu)(1-2\nu)}\left[\frac{C_1(1-2\nu)}{r^2} + C_2 + \varepsilon_0\nu\right] - \frac{r^2\omega^2(1+2\nu)\rho}{8(1-\nu)} - \frac{E\alpha}{r^2(1-\nu)}\left[r^2T(r) - \int_a^r \lambda T(\lambda)\mathrm{d}\lambda\right] \tag{30}$$

The above expressions for the radial displacement and radial and circumferential stresses are also given in Ref. (Apatay and Mack 2015). The stress in the axial direction can be calculated using Eqs. (26), (29), and (30) which yields

$$\sigma_z = \frac{E}{(1+\nu)(1-2\nu)}\left[2C_2\nu + \varepsilon_0(1-\nu)\right] - \frac{r^2\omega^2\nu\rho}{2(1-\nu)} - \frac{E\alpha T(r)}{(1-\nu)} \tag{31}$$

The solution is completed by calculating the integration constants and the axial strain ε_0. The boundary conditions for internally pressurized inner surface and stress-free outer surface can be written as

$$\sigma_r(a) = -P \text{ and } \sigma_r(b) = 0 \tag{32}$$

where P is the pressure at the inner surface. In addition, in case of generalized plane strain, the net force in the axial direction vanishes since the ends of the tube are free. This gives the following equation:

$$2\pi\int_a^b \sigma_z(r)r\mathrm{d}r = 0 \tag{33}$$

Using these conditions, the integration constants and the axial strain are obtained as

$$C_1 = \frac{a^2b^2P(1+\nu)}{(b^2-a^2)E} + \frac{a^2b^2\omega^2\rho(1+\nu)(3-2\nu)}{8E(1-\nu)} + \frac{a^2\alpha(1+\nu)}{(b^2-a^2)(1-\nu)}\int_a^b \lambda T(\lambda)\mathrm{d}\lambda \tag{34}$$

$$C_2 = \frac{a^2P(1-\nu)}{(b^2-a^2)E} + \frac{(a^2+b^2)\omega^2\rho(3-5\nu)}{8E(1-\nu)} + \frac{\alpha(1-3\nu)}{(b^2-a^2)(1-\nu)}\int_a^b \lambda T(\lambda)\mathrm{d}\lambda \tag{35}$$

$$\varepsilon_0 = \frac{2a^2P\nu}{(b^2-a^2)E} - \frac{(a^2+b^2)\omega^2\rho\nu}{2E} + \frac{2\alpha}{b^2-a^2}\int_a^b \lambda T(\lambda)\mathrm{d}\lambda \tag{36}$$

For the two-layer composite tubes with free ends, the same displacement and stress expressions given in Eqs. (28) to (31) are valid, and these expressions include four unknown integration constants: C_1, C_2 for the inner tube, and C_3, C_4 for the outer tube. In addition, the axial strain ε_0 should also be determined. In the derivations, the subscripts 1 and 2 are employed to represent material properties (α ,E,ν and ρ) of the inner and outer tubes, respectively, and superscripts I and II stand for the inner and outer tubes. The boundary conditions for the two-layer composite tubes under internal pressure are $\sigma_r^I(a) = -P$ and $\sigma_r^{II}(b) = 0$. In addition, at the interface of the two tubes (at $r = r_1$) the radial stress and radial displacement must be continuous, and thus, one can write $\sigma_r^I(r_1) = \sigma_r^{II}(r_1)$ and $u^I(r_1) = u^{II}(r_1)$. Moreover, for the generalized plane strain case one can write

$$2\pi\int_a^{r_1}\sigma_z^I(r)r\mathrm{d}r + 2\pi\int_{r_1}^b \sigma_z^{II}(r)r\mathrm{d}r = 0 \tag{37}$$

Substituting the stresses and displacements into these conditions, the following system of equations is obtained:

$$\begin{bmatrix} \frac{1}{r_1} & r_1 & -\frac{1}{r_1} & -r_1 & 0 \\ -\frac{E_1}{r_1^2(1+\nu_1)} & \frac{E_1}{(1+\nu_1)(1-2\nu_1)} & \frac{E_2}{r_1^2(1+\nu_2)} & -\frac{E_2}{(1+\nu_2)(1-2\nu_2)} & K_{25} \\ -\frac{E_1}{a^2(1+\nu_1)} & \frac{E_1}{(1+\nu_1)(1-2\nu_1)} & 0 & 0 & \frac{E_1\nu_1}{(1+\nu_1)(1-2\nu_1)} \\ 0 & 0 & -\frac{E_2}{b^2(1+\nu_2)} & \frac{E_2}{(1+\nu_2)(1-2\nu_2)} & \frac{E_2\nu_2}{(1+\nu_2)(1-2\nu_2)} \\ 0 & \frac{2(r_1^2-a^2)E_1\nu_1}{(1+\nu_1)(1-2\nu_1)} & 0 & \frac{2(b^2-r_1^2)E_2\nu_2}{(1+\nu_2)(1-2\nu_2)} & K_{55} \end{bmatrix} \begin{bmatrix} C_1 \\ C_2 \\ C_3 \\ C_4 \\ \varepsilon_0 \end{bmatrix} = \begin{bmatrix} B_1 \\ B_2 \\ B_3 \\ B_4 \\ B_5 \end{bmatrix} \tag{38}$$

where

$$K_{25} = \frac{E_1\nu_1}{(1+\nu_1)(1-2\nu_1)} - \frac{E_2\nu_2}{(1+\nu_2)(1-2\nu_2)} \tag{39}$$

$$K_{55} = \frac{(r_1^2-a^2)E_1(1-\nu_1)}{(1+\nu_1)(1-2\nu_1)} + \frac{(b^2-r_1^2)E_2(1-\nu_2)}{(1+\nu_2)(1-2\nu_2)} \tag{40}$$

$$B_1 = \frac{r_1^3\omega^2}{8}\left[\frac{(1+\nu_1)(1-2\nu_1)\rho_1}{E_1(1-\nu_1)} - \frac{(1+\nu_2)(1-2\nu_2)\rho_2}{E_2(1-\nu_2)}\right] - \frac{\alpha_1(1+\nu_1)}{r_1(1-\nu_1)}\int_a^{r_1}\lambda T_1(\lambda)\mathrm{d}\lambda \tag{41}$$

$$B_2 = \frac{r_1^2\omega^2}{8}\left[\frac{(3-2\nu_1)\rho_1}{1-\nu_1} - \frac{(3-2\nu_2)\rho_2}{1-\nu_2}\right] + \frac{E_1\alpha_1}{r_1^2(1-\nu_1)}\int_a^{r_1}\lambda T_1(\lambda)\mathrm{d}\lambda \tag{42}$$

$$B_3 = \frac{a^2\omega^2(3-2\nu_1)\rho_1}{8(1-\nu_1)} - P \tag{43}$$

$$B_4 = \frac{b^2\omega^2(3-2\nu_2)\rho_2}{8(1-\nu_2)} + \frac{E_2\alpha_2}{b^2(1-\nu_2)}\int_{r_1}^b \lambda T_2(\lambda)\mathrm{d}\lambda \tag{44}$$

$$B_5 = \frac{\omega^2}{4}\left[\frac{(r_1^4 - a^4)\nu_1\rho_1}{1-\nu_1} + \frac{(b^4 - r_1^4)\nu_2\rho_2}{1-\nu_2}\right] + \frac{2E_1\alpha_1}{1-\nu_1}\int_a^{r_1} \lambda T_1(\lambda)d\lambda + \frac{2E_2\alpha_2}{1-\nu_2}\int_{r_1}^{b} \lambda T_2(\lambda)\mathrm{d}\lambda \tag{45}$$

The integration constants and the axial strain can be obtained by solving Eq. (38).

Similar to two-layer composite tubes, the same displacement and stress expressions [Eqs. (28)–(31)] are valid for the three-layer tubes. The foregoing expressions contain six unknown integration constants (C_1,C_2 for the inner tube, C_3, C_4 for the middle tube, and C_5, C_6 for the outer tube) and the axial strain ε_0. The subscripts 1, 2, and 3 are employed to represent material properties of the inner, middle, and outer tubes, respectively. Moreover, superscripts I, II, and III are used to determine the displacements and stresses developed in the inner, middle, and outer tubes. The boundary conditions for the three-layer composite tubes under internal pressure are $\sigma_r^I(a) = -P$ and $\sigma_r^{III}(b) = 0$. In addition, at the interfaces of the tubes the radial stresses and radial displacements must be continuous, and one can write $\sigma_r^I(r_1) = \sigma_r^{II}(r_1)$, $u^I(r_1) = u^{II}(r_1)$, $\sigma_r^{II}(r_2) = \sigma_r^{III}(r_2)$ and $u^{II}(r_2) = u^{III}(r_2)$. Finally, for the generalized plane strain state, one can write

$$2\pi\int_a^{r1} \sigma_z^I(r)r\mathrm{d}r + 2\pi\int_{r1}^{r2} \sigma_z^{II}(r)r\mathrm{d}r + 2\pi\int_{r2}^{b} \sigma_z^{III}(r)r\mathrm{d}r = 0 \tag{46}$$

Using the above equation and the boundary and interface conditions, the following system of equations can be obtained:

$$\begin{bmatrix} \frac{1}{r_1} & r_1 & -\frac{1}{r_1} & -r_1 & 0 & 0 & 0 \\ 0 & 0 & \frac{1}{r_2} & r_2 & -\frac{1}{r_2} & -r_2 & 0 \\ -\frac{E_1}{r_1^2(1+\nu_1)} & K_{32} & \frac{E_2}{r_1^2(1+\nu_2)} & K_{34} & 0 & 0 & K_{37} \\ 0 & 0 & -\frac{E_2}{r_2^2(1+\nu_2)} & K_{44} & \frac{E_3}{r_2^2(1+\nu_3)} & K_{46} & K_{47} \\ \frac{E_1}{a^2(1+\nu_1)} & K_{52} & 0 & 0 & 0 & 0 & K_{57} \\ 0 & 0 & 0 & 0 & -\frac{E_3}{b^2(1+\nu_3)} & K_{66} & K_{67} \\ 0 & K_{72} & 0 & K_{74} & 0 & K_{76} & K_{77} \end{bmatrix} \begin{bmatrix} C_1 \\ C_2 \\ C_3 \\ C_4 \\ C_5 \\ C_6 \\ \varepsilon_0 \end{bmatrix} = \begin{bmatrix} B_1 \\ B_2 \\ B_3 \\ B_4 \\ B_5 \\ B_6 \\ B_7 \end{bmatrix} \tag{47}$$

where $K_{32} = K_{52} = \frac{E_1}{(1+\nu_1)(1-2\nu_1)}$, $K_{34} = K_{44} = \frac{E_2}{(1+\nu_2)(1-2\nu_2)}$, $K_{37} = K_{32}\nu_1 - K_{34}\nu_2$, $K_{46} = -K_{66} = -\frac{E_3}{(1+\nu_3)(1-2\nu_3)}$, $K_{47} = K_{34}\nu_2 + K_{46}$, $K_{57} = K_{32}\nu_1$, $K_{67} = -K_{46}\nu_3$, $K_{72} = \frac{2(r_1^2-a^2)E_1\nu_1}{(1+\nu_1)(1-2\nu_1)}$, $K_{74} = \frac{2(r_2^2-r_1^2)E_2\nu_2}{(1+\nu_2)(1-2\nu_2)}$, $K_{76} = \frac{2(b^2-r_2^2)E_3\nu_3}{(1+\nu_3)(1-2\nu_3)}$,

$$K_{77} = \frac{(r_1^2 - a^2)E_1(1-\nu_1)}{(1+\nu_1)(1-2\nu_1)} + \frac{(r_2^2 - r_1^2)E_2(1-\nu_2)}{(1+\nu_2)(1-2\nu_2)} + \frac{(b^2 - r_1^2)E_3(1-\nu_3)}{(1+\nu_3)(1-2\nu_3)} \tag{48}$$

and

$$B_1 = \frac{r_1^3\omega^2}{8}\left[\frac{(1+\nu_1)(1-2\nu_1)\rho_1}{E_1(1-\nu_1)} - \frac{(1+\nu_2)(1-2\nu_2)\rho_2}{E_2(1-\nu_2)}\right] - \frac{\alpha_1(1+\nu_1)}{r_1(1-\nu_1)}\int_a^{r_1} \lambda T_1(\lambda)\mathrm{d}\lambda \tag{49}$$

$$B_2 = \frac{r_2^3\omega^2}{8}\left[\frac{(1+\nu_2)(1-2\nu_2)\rho_2}{E_2(1-\nu_2)} - \frac{(1+\nu_3)(1-2\nu_3)\rho_3}{E_3(1-\nu_3)}\right] - \frac{\alpha_2(1+\nu_2)}{r_2(1-\nu_2)}\int_{r_1}^{r_2} \lambda T_2(\lambda)\mathrm{d}\lambda \tag{50}$$

$$B_3 = \frac{r_1^2\omega^2}{8}\left[\frac{(3-2\nu_1)\rho_1}{1-\nu_1} - \frac{(3-2\nu_2)\rho_2}{1-\nu_2}\right] + \frac{E_1\alpha_1}{r_1^2(1-\nu_1)}\int_a^{r_1} \lambda T_1(\lambda)\mathrm{d}\lambda \tag{51}$$

$$B_4 = \frac{r_2^2\omega^2}{8}\left[\frac{(3-2\nu_2)\rho_2}{1-\nu_2} - \frac{(3-2\nu_3)\rho_3}{1-\nu_3}\right] + \frac{E_2\alpha_2}{r_2^2(1-\nu_2)}\int_{r_1}^{r_2} \lambda T_2(\lambda)\mathrm{d}\lambda \tag{52}$$

$$B_5 = \frac{a^2\omega^2(3-2\nu_1)\rho_1}{8(1-\nu_1)} - P \tag{53}$$

$$B_6 = \frac{b^2\omega^2(3-2\nu_3)\rho_3}{8(1-\nu_3)} + \frac{E_3\alpha_3}{b^2(1-\nu_3)}\int_{r_2}^{b} \lambda T_3(\lambda)\mathrm{d}\lambda \tag{54}$$

$$B_7 = \frac{\omega^2}{4}\left[\frac{(r_1^4 - a^4)\nu_1\rho_1}{1-\nu_1} + \frac{(r_2^4 - r_1^4)\nu_2\rho_2}{1-\nu_2} + \frac{(b^4 - r_2^4)\nu_3\rho_3}{1-\nu_2}\right] + \frac{2E_1\alpha_1}{1-\nu_1}\int_a^{r_1}\lambda T_1(\lambda)\mathrm{d}\lambda + \frac{2E_2\alpha_2}{1-\nu_2}\int_{r_1}^{r_2}\lambda T_2(\lambda)\mathrm{d}\lambda + \frac{2E_3\alpha_3}{1-\nu_3}\int_{r_2}^{b}\lambda T_3(\lambda)\mathrm{d}\lambda \tag{55}$$

2.2.2 Plane Strain Case (Fixed Ends)

The solution for a single-layer tube with axially constrained ends is obtained through setting $\varepsilon_z = 0$. The stress components in radial, circumferential, and axial directions can be obtained as

$$\sigma_r = \frac{E}{(1+\nu)(1-2\nu)}\left[-\frac{C_1(1-2\nu)}{r^2} + C_2\right] - \frac{r^2\omega^2(3-2\nu)\rho}{8(1-\nu)} - \frac{E\alpha}{r^2(1-\nu)}\int_a^r \lambda T(\lambda)\mathrm{d}\lambda \tag{56}$$

$$\sigma_\theta = \frac{E}{(1+\nu)(1-2\nu)}\left[\frac{C_1(1-2\nu)}{r^2} + C_2\right]\frac{r^2\omega^2(1+2\nu)\rho}{8(1-\nu)} - \frac{E\alpha}{r^2(1-\nu)}\left[r^2T(r) - \int_a^r \lambda T(\lambda)\mathrm{d}\lambda\right] \tag{57}$$

$$\sigma_z = \frac{2EC_2\nu}{(1+\nu)(1-2\nu)} - \frac{r^2\omega^2\nu\rho}{2(1-\nu)} - \frac{E\alpha T(r)}{(1-\nu)} \tag{58}$$

On the other hand, the radial displacement is the same as the expression given in Eq. (28). By using the boundary conditions given in Eq. (32), the integration constants C_1 and C_2 can be determined as

$$C_1 = \frac{a^2b^2P(1+\nu)}{(b^2-a^2)E} + \frac{a^2b^2\omega^2\rho(1+\nu)(3-2\nu)}{8E(1-\nu)} + \frac{a^2\alpha(1+\nu)}{(b^2-a^2)(1-\nu)}\int_a^b rT(r)\mathrm{d}r \tag{59}$$

$$C_2 = \frac{a^2P(1-\nu)(1-2\nu)}{(b^2-a^2)E} + \frac{(a^2+b^2)\omega^2\rho(1+\nu)(3-2\nu)(1-2\nu)}{8E(1-\nu)} + \frac{\alpha(1+\nu)(1-2\nu)}{(b^2-a^2)(1-\nu)}\int_a^b rT(r)\mathrm{d}r \tag{60}$$

For the two-layer tubes, the same stress and displacement expressions for axially constrained single-layer tubes are valid and the integration constants can be determined by the boundary and interface conditions formerly expressed for the two-layer tubes having free ends. Using these conditions, they can be determined by solving the following system of equations:

$$\begin{bmatrix} \frac{1}{r_1} & r_1 & -\frac{1}{r_1} & -r_1 \\ -\frac{E_1}{r_1^2(1+\nu_1)} & \frac{E_1}{(1+\nu_1)(1-2\nu_1)} & \frac{E_2}{r_1^2(1+\nu_2)} & -\frac{E_2}{(1+\nu_2)(1-2\nu_2)} \\ -\frac{E_1}{a^2(1+\nu_1)} & \frac{E_1}{(1+\nu_1)(1-2\nu_1)} & 0 & 0 \\ 0 & 0 & -\frac{E_2}{b^2(1+\nu_2)} & \frac{E_2\nu_2}{(1+\nu_2)(1-2\nu_2)} \end{bmatrix}\begin{bmatrix} C_1 \\ C_2 \\ C_3 \\ C_4 \end{bmatrix} = \begin{bmatrix} B_1 \\ B_2 \\ B_3 \\ B_3 \end{bmatrix} \tag{61}$$

where B_2, B_3 and B_4 are given in Eqs. (41)–(44).

Finally, for the three-layer fixed-ended tubes, similar to the two-layer tubes with fixed ends, the six integration constants are to be determined using the following system of equations:

$$\begin{bmatrix} \frac{1}{r_1} & r_1 & -\frac{1}{r_1} & -r_1 & 0 & 0 \\ 0 & 0 & \frac{1}{r_2} & r_2 & -\frac{1}{r_2} & -r_2 \\ -\frac{E_1}{r_1^2(1+\nu_1)} & K_{32} & \frac{E_2}{r_1^2(1+\nu_2)} & K_{34} & 0 & 0 \\ 0 & 0 & -\frac{E_2}{r_2^2(1+\nu_2)} & K_{44} & \frac{E_3}{r_2^2(1+\nu_3)} & K_{46} \\ \frac{E_1}{a^2(1+\nu_1)} & K_{52} & 0 & 0 & 0 & 0 \\ 0 & 0 & 0 & 0 & -\frac{E_3}{b^2(1+\nu_3)} & K_{66} \end{bmatrix} \begin{bmatrix} C_1 \\ C_2 \\ C_3 \\ C_4 \\ C_5 \\ C_6 \end{bmatrix} = \begin{bmatrix} B_1 \\ B_2 \\ B_3 \\ B_4 \\ B_5 \\ B_6 \end{bmatrix} \tag{62}$$

where K_{32}, K_{34}, K_{44}, K_{46}, K_{52}, K_{66}, B_1, B_2, B_3, B_4, B_5 and B_6 are already given in Eqs. (48)–(54).

2.3 Onset of Yield

Monitoring the commencement of yielding for a tube with fixed or free ends is quite important in order to perform a reliable design. For an internally pressurized single-layer tube, typically, the yielding begins at the inner surface ($r=a$). It is also known that for the fixed-ended two-layer tubes, depending on material properties and tube dimensions, the yielding may occur in the inner surface or at the interfaces of tube layers (Akis and Eraslan 2005; Eraslan and Akis 2005). On the other hand, when the temperature load and rotation are considered, the plasticization may also start at the outer surface of the tube assemblies with free ends (Apatay and Mack 2015). Therefore, all these locations, together with the inner parts of the layers, should be checked for yielding. To do this, the well-known von Mises yield criterion is used in this work. The von Mises yield stress σ_Y can be stated as

$$\sigma_Y = \sqrt{\frac{1}{2}[(\sigma_r - \sigma_\theta)^2 + (\sigma_r - \sigma_z)^2 + (\sigma_\theta - \sigma_z)^2]}. \tag{63}$$

The yielding takes place once the yield stress σ_Y becomes higher than the uniaxial yield limit σ_0 of the material. For determining the yielding at the layers of the assemblies, the following non-dimensional yield variable is expressed with respect to the von Mises yield stress:

$$\varphi = \sqrt{\frac{1}{2}[(\bar{\sigma}_r - \bar{\sigma}_\theta)^2 + (\bar{\sigma}_r - \bar{\sigma}_z)^2 + (\bar{\sigma}_\theta - \bar{\sigma}_z)^2]}, \tag{64}$$

where $\bar{\sigma}_i$ are the non-dimensional stress components determined by

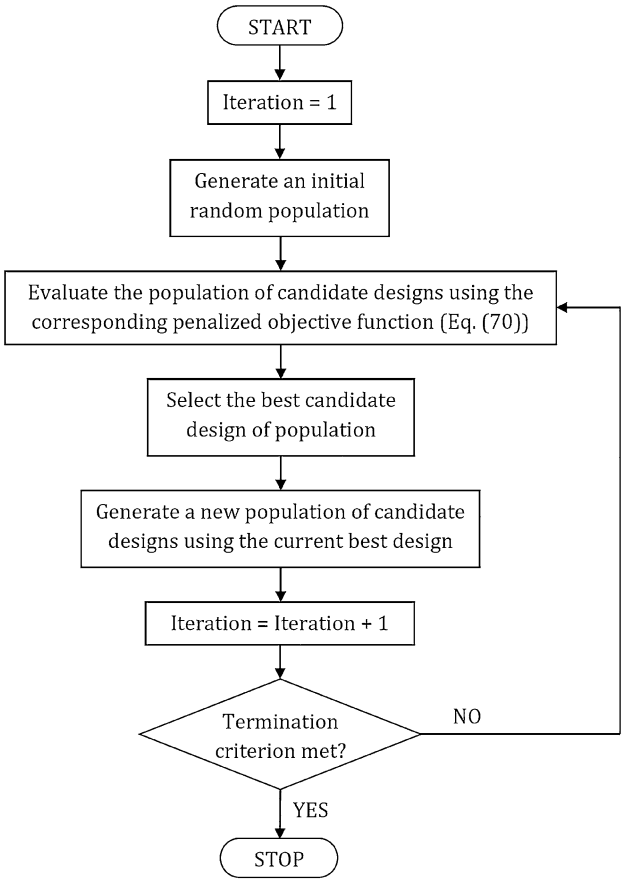

Fig. 2 Flowchart of the metaheuristic optimization algorithm

$$\bar{\sigma}_i = \frac{\sigma_i}{\sigma_0} \tag{65}$$

It is worth noting that for the values of $\varphi < 1$, the assembly is in elastic stress state, whereas for $\varphi = 1$, the yielding begins at that location. In the computations, the yield variable is calculated throughout the assemblies where yielding may occur.

3 Optimal Design Problem Formulation

The present section provides the mathematical formulation of the considered combinatorial optimization problem. The weight minimization problem of a multilayer composite tube with *nl* material layers and *nv* number of solution variables, including thickness and material variables, can be formulated as follows.

$$\text{Find } \mathbf{X}^T = [x_1, x_2, \ldots, x_{nv}] \tag{66}$$

such that $\boldsymbol{X}$ minimizes the following weight objective function:

Table 1 Material properties and costs of the available steel (S) and aluminum (A) alloys

Material	Designation	E (GPa)	ν	σ_0 (MPa)	ρ (ton/m^3)	k (W/m °C)	α (10^{-6}/ °C)	Cost ($/ton)
1	S-1	193	0.27	207	7.86	35	11.8	7000
2	S-2	193	0.27	280	7.92	41	12.0	8000
3	S-3	200	0.29	390	7.85	28	11.9	8500
4	S-4	200	0.32	703	8.16	32	12.3	9000
5	S-5	193	0.27	760	7.92	30	11.7	9500
6	A-1	70	0.33	103	2.71	210	23.0	4000
7	A-2	68.9	0.33	145	2.71	170	22.8	4300
8	A-3	68.9	0.35	255	2.71	185	23.2	4500
9	A-4	74.5	0.33	320	2.77	190	23.5	5000
10	A-5	73.1	0.35	414	2.79	200	22.9	5500

$$W(X) = \sum_{i=1}^{nl} \rho_i A_i \tag{67}$$

where $W(X)$ is the weight per unit length of the tube. In the above equation, ρ_i and A_i are weight per unit of volume and cross-sectional area of the i-th material layer, respectively. On the other hand, for cost optimization, minimization of the following cost objective function is considered:

$$C(X) = \sum_{i=1}^{nl} c_i \rho_i A_i \tag{68}$$

where $C(X)$ is the cost per unit length of the tube. Here, ρ_i, c_i, and A_i are weight per unit of volume, cost per unit weight, and cross-sectional area of the i-th material layer, respectively. In the present study, both the minimum weight and cost design of rotating multilayer tubes are subjected to the following design constraint:

$$\phi_i - 1 < 0 \tag{69}$$

where φ_i is non-dimensional stress variable defined by Eq. (64). During the optimization process, weight and cost objective function values of the feasible designs are directly calculated by Eqs. (67) and (68), respectively. However, infeasible designs are penalized as follows.

$$f_p(X) = f(X)\left[1 + K\left(\sum_i g_i\right)\right] \tag{70}$$

where $f(X)$ is the associated weight/cost objective function, $f_p(X)$ denotes the penalized objective function, g_i is the i-th constraint violation, and K is the penalty constant, which is taken as 100 in this study.

4 Metaheuristic Optimization Algorithm

Selection of a suitable algorithm to solve a particular design optimization problem basically depends on the nature of design variables, objective function, and imposed constraints. Metaheuristic or evolutionary algorithms are generally perceived as efficient numerical optimization methods for engineering design applications (Akbulut et al. 2020; Kazemzadeh Azad 2019). The popularity of these algorithms in practical applications (Koç 2017; Alkayem et al. 2018; Gen et al. 2017) can be attributed to their ease of implementation, derivative-free features, global search properties, and capability of dealing with both discrete and continuous solution variables.

Considering the discrete nature of the problem tackled in the present study, a reformulation of the big bang-big crunch algorithm (Erol and Eksin 2006), recently proposed by Kazemzadeh Azad and Akış (2018), is adopted for design optimization of rotating multilayer composite tubes. Akin to other metaheuristic algorithms, optimization via big bang-big crunch algorithm begins with an initial population of candidate solutions that are uniformly sampled from the design space. Next, evaluation, selection, and generation processes are carried out successively to create a new population of candidate solutions. As shown in the flowchart of the optimization method (Fig. 2), the algorithm entails an iterative process to obtain the optimum thickness and material of each layer for a given composite tube under the imposed design constraints. It is worth mentioning that, to satisfy the fabrication requirements, the thickness of each material layer is rounded to the nearest available value in the course of optimization. The algorithm is coded in MATLAB (MATLAB 2019), and the optimization runs are performed using a regular personal computer with Intel Core i5-8250U, 1.6 GHz CPU, and 8 GB RAM. Further details for the implementation of the employed big bang-big crunch algorithm can be found in Ref. (Kazemzadeh Azad and Akış 2018) and are not repeated here.

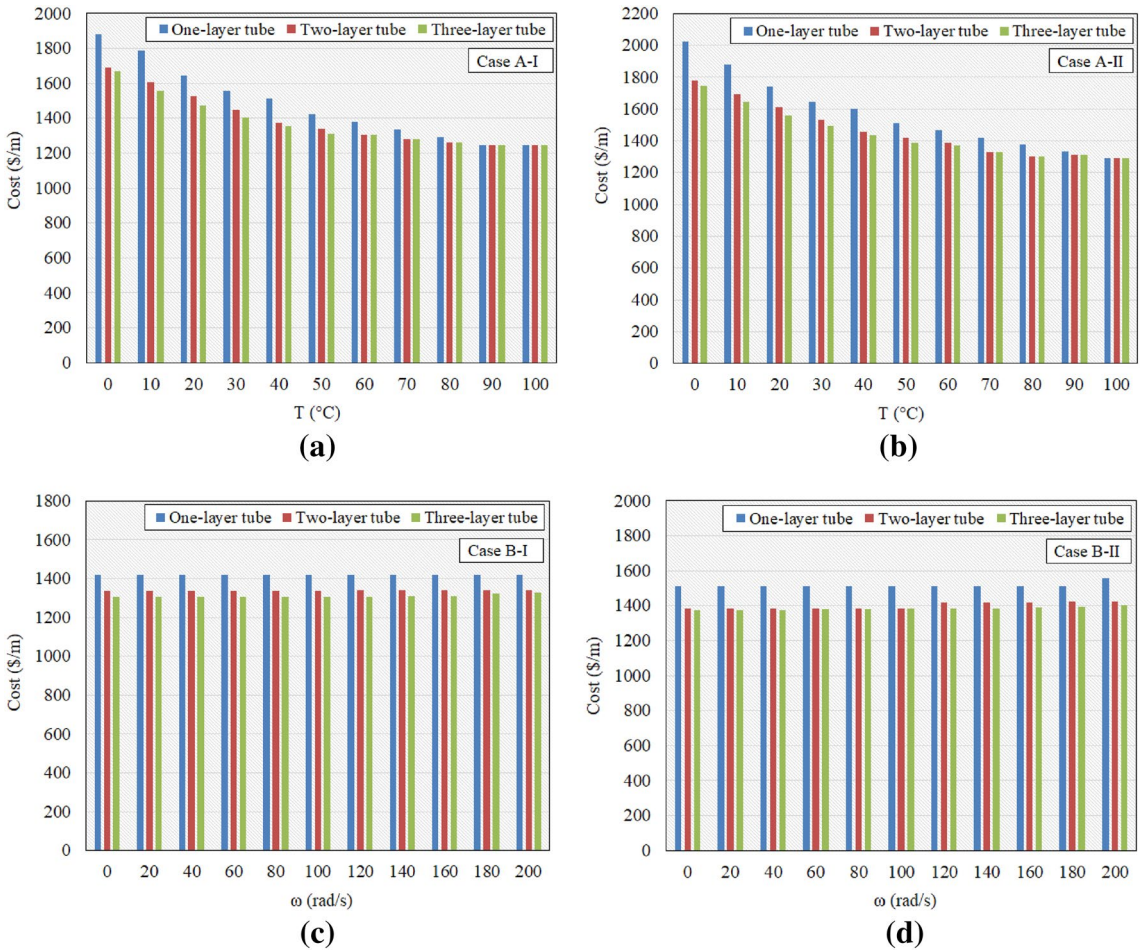

Fig. 3 Optimum costs for rotating one-, two-, and three-layer tubes: **a** Case A-I; **b** Case A-II; **c** Case B-I; and **d** Case B-II

Table 2 Cost minimization results of rotating three-layer tube in Case A-I

T (°C)	A (m)	R_1 (m)	R_2 (m)	B (m)	Layer$_1$	Layer$_2$	Layer$_3$	$\Phi_{(c)}$	Best cost ($/m)	Worst cost	Mean cost	Standard deviation
100	0.15	0.164	0.212	0.22	A-5	A-5	A-5	0.9829	1248.6	1321.7	1251.5	14.6
90	0.15	0.194	0.202	0.22	A-5	A-5	A-5	0.9950	1248.6	1486.0	1261.7	47.8
80	0.15	0.17	0.206	0.222	A-5	A-5	A-4	0.9980	1259.0	1259.0	1259.0	0
70	0.15	0.182	0.196	0.224	A-5	A-5	A-4	0.9977	1279.0	1279.0	1279.0	0
60	0.15	0.19	0.222	0.226	A-5	A-4	A-4	0.9942	1307.2	1307.2	1307.2	0
50	0.15	0.186	0.216	0.228	A-5	A-4	A-3	0.9988	1312.0	1339.7	1313.1	5.5
40	0.15	0.182	0.206	0.232	A-5	A-4	A-3	0.9977	1353.6	1372.6	1354.8	4.0
30	0.15	0.178	0.2	0.236	A-5	A-4	A-3	0.9999	1405.9	1446.6	1412.7	15.2
20	0.15	0.176	0.198	0.24	A-5	A-4	A-3	0.9995	1471.4	1531.5	1478.5	19.2
10	0.15	0.174	0.204	0.244	A-5	A-4	A-3	0.9997	1554.8	1614.0	1564.6	22.0
0	0.15	0.174	0.204	0.25	A-5	A-4	A-3	0.9993	1668.4	1733.7	1686.5	27.1

Table 3 Cost-minimization results of rotating three-layer tube in Case A-II

T (°C)	A (m)	R_1 (m)	R_2 (m)	B (m)	Layer$_1$	Layer$_2$	Layer$_3$	$\Phi_{(c)}$	Best cost ($/m)	Worst cost	Mean cost	Standard deviation
100	0.15	0.198	0.204	0.222	A-5	A-5	A-5	0.9834	1291.2	1540.9	1311.0	53.1
90	0.15	0.2	0.214	0.224	A-5	A-5	A-4	0.9980	1313.6	1313.6	1313.6	0
80	0.15	0.208	0.214	0.224	A-5	A-4	A-4	0.9988	1301.7	1301.7	1301.7	0
70	0.15	0.188	0.2	0.226	A-5	A-5	A-4	0.9983	1325.6	1325.6	1325.6	0
60	0.15	0.19	0.224	0.23	A-5	A-4	A-3	0.9997	1372.4	1372.4	1372.4	0
50	0.15	0.188	0.216	0.232	A-5	A-4	A-3	0.9991	1386.0	1419.8	1395.4	15.5
40	0.15	0.184	0.208	0.236	A-5	A-4	A-3	0.9988	1433.1	1456.8	1435.9	7.9
30	0.15	0.182	0.204	0.24	A-5	A-4	A-3	0.9992	1494.0	1555.1	1500.2	15.5
20	0.15	0.178	0.22	0.242	A-5	A-4	A-3	0.9999	1559.5	1614.0	1564.0	14.8
10	0.15	0.176	0.21	0.248	A-5	A-4	A-3	0.9990	1646.4	1712.7	1652.1	18.3
0	0.15	0.174	0.222	0.252	A-5	A-4	A-3	0.9993	1746.7	1827.2	1753.5	21.6

Table 4 Cost-minimization results of rotating three-layer tube in Case B-I

ω (rad/s)	A (m)	R_1 (m)	R_2 (m)	B (m)	Layer$_1$	Layer$_2$	Layer$_3$	$\Phi_{(c)}$	Best cost ($/m)	Worst cost	Mean cost	Standard deviation
200	0.15	0.186	0.222	0.228	A-5	A-4	A-3	0.9997	1325.7	1339.7	1330.7	6.9
180	0.15	0.186	0.22	0.228	A-5	A-4	A-3	0.9989	1321.1	1339.7	1324.8	7.6
160	0.15	0.186	0.216	0.228	A-5	A-4	A-3	0.9996	1312.0	1339.7	1316.4	10.4
140	0.15	0.186	0.216	0.228	A-5	A-4	A-3	0.9979	1312.0	1339.7	1318.6	12.1
120	0.15	0.186	0.214	0.228	A-5	A-4	A-3	0.9994	1307.5	1339.7	1316.5	14.7
100	0.15	0.186	0.214	0.228	A-5	A-4	A-3	0.9983	1307.5	1360.1	1314.2	14.3
80	0.15	0.186	0.214	0.228	A-5	A-4	A-3	0.9973	1307.5	1336.2	1309.8	7.9
60	0.15	0.186	0.214	0.228	A-5	A-4	A-3	0.9966	1307.5	1336.2	1312.1	10.7
40	0.15	0.186	0.214	0.228	A-5	A-4	A-3	0.9961	1307.5	1336.2	1311.0	9.5
20	0.15	0.186	0.214	0.228	A-5	A-4	A-3	0.9958	1307.5	1336.2	1308.7	5.7
0	0.15	0.186	0.214	0.228	A-5	A-4	A-3	0.9957	1307.5	1336.2	1314.4	12.5

Table 5 Cost-minimization results of rotating three-layer tube in Case B-II

ω (rad/s)	A (m)	R_1 (m)	R_2 (m)	B (m)	Layer$_1$	Layer$_2$	Layer$_3$	$\Phi_{(c)}$	Best cost ($/m)	Worst cost	Mean cost	Standard deviation
200	0.15	0.188	0.224	0.232	A-5	A-4	A-3	0.9988	1404.3	1423.3	1407.0	6.4
180	0.15	0.188	0.22	0.232	A-5	A-4	A-3	0.9992	1395.1	1423.3	1398.4	9.4
160	0.15	0.188	0.218	0.232	A-5	A-4	A-3	0.9986	1390.5	1419.8	1394.0	9.7
140	0.15	0.188	0.216	0.232	A-5	A-4	A-3	0.9982	1386.0	1419.8	1390.0	11.2
120	0.15	0.188	0.216	0.232	A-5	A-4	A-3	0.9965	1386.0	1448.7	1392.6	16.2
100	0.15	0.188	0.198	0.23	A-5	A-4	A-4	0.9995	1383.1	1386.0	1383.2	0.6
80	0.15	0.188	0.228	0.23	A-5	A-4	A-3	0.9998	1378.3	1383.1	1380.2	2.4
60	0.15	0.188	0.228	0.23	A-5	A-4	A-3	0.9989	1378.3	1383.1	1380.8	2.4
40	0.15	0.188	0.226	0.23	A-5	A-4	A-3	0.9997	1373.6	1383.1	1377.0	4.6
20	0.15	0.188	0.226	0.23	A-5	A-4	A-3	0.9994	1373.6	1439.1	1380.4	13.1
0	0.15	0.188	0.226	0.23	A-5	A-4	A-3	0.9992	1373.6	1383.1	1378.1	4.8

5 Numerical Experiments

This section presents the weight and cost optimization instances of rotating multilayer composite tubes under internal heating and pressure. Table 1 gives the set of available steel and aluminum alloys used for material selection of the composite tube layers. This set of steel and aluminum alloys was formerly adopted in Ref. (Kazemzadeh Azad and Akış 2018) for the optimal design of internally pressurized tightly fitted multilayer composite tubes with axially constrained ends. In the present work, both weight and cost optimization examples of internally pressurized multilayer composite tubes are investigated for different angular speed and inner surface temperature values, and the obtained results are presented and discussed. The numerical instances are studied in two different cases, i.e., Case A and Case B, as follows.

In Case A, it is aimed to examine the effect of internal heating on the final designs. For this purpose, angular speed and internal pressure of the composite tubes are set to $\omega = 150$ rad/s and $P = 150$ MPa, respectively, while the internal temperature of the assemblies, T, is gradually increased from 0 to 100 °C. Here, using the aforementioned metaheuristic optimization algorithm the corresponding optimum design for each temperature value is sought and the obtained solutions are compared. In Case B, it is attempted to investigate the effect of angular speed of the assemblies on the final results. To this end, internal temperature and pressure are set to $T = 50$ °C and $P = 150$ MPa, respectively, while the angular speed of the assemblies, ω, is gradually increased from 0 to 200 rad/s. The optimum design associated with each angular speed value is sought, and the final designs are reported.

Moreover, all the numerical examples are further investigated under two different end conditions already described in Sect. 2. The optimization of assemblies with axially constrained ends (fixed-end assumption) is denoted by Case I, whereas the optimal design of composite tubes considering the generalized plane strain formulation (free-end assumption) is denoted by Case II. To investigate the effect of number of material layers on the final solutions, the numerical experiments are carried out for all the one-,

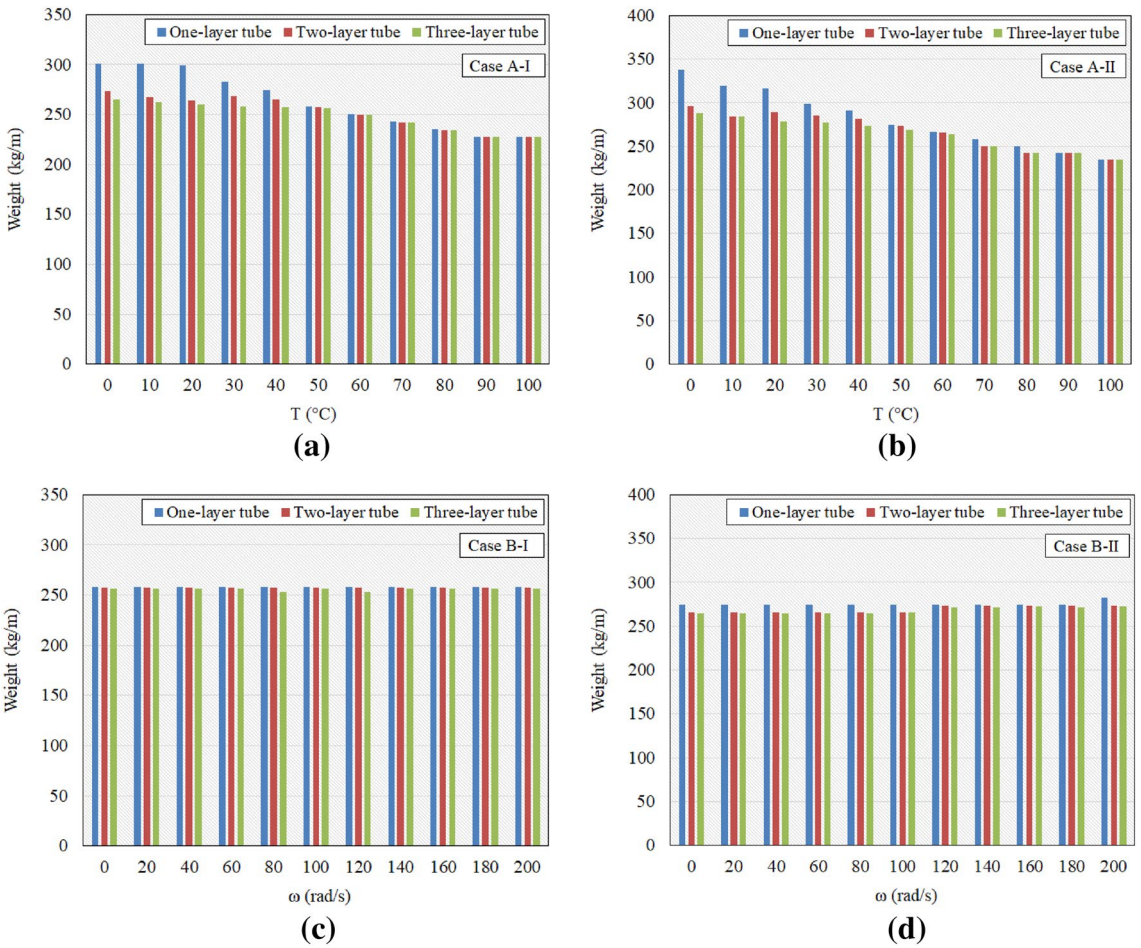

Fig. 4 Optimum weights for rotating one-, two-, and three-layer tubes: **a** Case A-I; **b** Case A-II; **c** Case B-I; and **d** Case B-II

Table 6 Weight-minimization results of rotating three-layer tube in Case A-I

T (°C)	A (m)	R_1 (m)	R_2 (m)	B (m)	Layer$_1$	Layer$_2$	Layer$_3$	$\Phi_{(c)}$	Best weight (kg/m)	Worst weight	Mean weight	Standard deviation
100	0.15	0.178	0.206	0.22	A-5	A-5	A-5	0.9829	227.0	255.5	233.8	12.3
90	0.15	0.2	0.204	0.22	A-5	A-5	A-5	0.9950	227.0	257.0	233.1	11.7
80	0.15	0.162	0.206	0.222	A-5	A-5	A-4	0.9980	234.3	260.4	236.4	7.2
70	0.15	0.196	0.206	0.224	A-5	A-4	A-4	0.9977	241.8	262.1	242.7	4.1
60	0.15	0.19	0.21	0.226	A-5	A-4	A-4	0.9942	249.5	266.7	250.2	3.4
50	0.15	0.186	0.216	0.228	A-5	A-4	A-3	0.9988	256.3	272.6	259.1	5.4
40	0.15	0.194	0.2	0.218	A-5	S-5	A-4	0.9974	257.0	275.4	264.7	4.1
30	0.15	0.186	0.196	0.212	A-5	S-5	A-4	0.9976	257.9	281.3	270.2	11.2
20	0.15	0.182	0.196	0.206	A-5	S-5	A-4	0.9979	259.8	295.8	280.7	16.0
10	0.15	0.176	0.192	0.204	A-5	S-5	A-4	0.9959	262.1	312.7	277.3	21.0
0	0.15	0.172	0.19	0.202	A-5	S-5	A-4	0.9989	265.2	331.3	279.9	19.4

Table 7 Weight-minimization results of rotating three-layer tube in Case A-II

T (°C)	A (m)	R_1 (m)	R_2 (m)	B (m)	Layer$_1$	Layer$_2$	Layer$_3$	$\Phi_{(c)}$	Best weight (kg/m)	Worst weight	Mean weight	Standard deviation
100	0.15	0.198	0.204	0.222	A-5	A-5	A-5	0.9834	234.8	271.9	239.8	12.5
90	0.15	0.166	0.214	0.224	A-5	A-5	A-4	0.9980	242.3	277.1	243.7	7.0
80	0.15	0.208	0.222	0.224	A-5	A-4	A-4	0.9988	242.1	282.6	243.8	8.1
70	0.15	0.192	0.2	0.226	A-5	A-5	A-4	0.9983	249.8	287.0	251.3	7.4
60	0.15	0.19	0.224	0.226	A-5	A-4	S-5	0.9985	264.1	290.0	265.2	5.2
50	0.15	0.206	0.21	0.224	A-5	S-5	A-4	0.9995	269.0	273.3	272.1	1.1
40	0.15	0.198	0.204	0.222	A-5	S-5	A-4	0.9995	273.2	301.0	280.7	4.9
30	0.15	0.194	0.202	0.22	A-5	S-5	A-4	0.9991	277.6	305.2	292.8	7.3
20	0.15	0.188	0.2	0.214	A-5	S-5	A-4	0.9999	278.9	313.8	296.7	15.5
10	0.15	0.176	0.182	0.202	A-5	A-4	S-5	0.9984	284.1	331.4	296.6	18.6
0	0.15	0.178	0.198	0.2	A-5	S-5	S-4	0.9999	288.0	347.8	305.4	25.5

Table 8 Weight-minimization results of rotating three-layer tube in Case B-I

ω (rad/s)	A (m)	R_1 (m)	R_2 (m)	B (m)	Layer$_1$	Layer$_2$	Layer$_3$	$\Phi_{(c)}$	Best weight (kg/m)	Worst weight	Mean weight	Standard deviation
200	0.15	0.186	0.222	0.228	A-5	A-4	A-3	0.9997	256.8	273.0	257.9	3.5
180	0.15	0.186	0.22	0.228	A-5	A-4	A-3	0.9989	256.7	274.4	257.6	3.5
160	0.15	0.186	0.216	0.228	A-5	A-4	A-3	0.9996	256.3	272.6	257.8	4.4
140	0.15	0.186	0.216	0.228	A-5	A-4	A-3	0.9979	256.3	271.0	257.4	3.7
120	0.15	0.2	0.204	0.22	A-5	S-5	A-4	0.9998	252.6	271.4	257.3	4.0
100	0.15	0.186	0.214	0.228	A-5	A-4	A-3	0.9983	256.2	268.7	257.2	3.3
80	0.15	0.2	0.204	0.22	A-5	S-5	A-4	0.9978	252.6	268.6	257.5	4.0
60	0.15	0.186	0.214	0.228	A-5	A-4	A-3	0.9966	256.2	268.9	257.3	3.5
40	0.15	0.186	0.214	0.228	A-5	A-4	A-3	0.9961	256.2	268.4	258.1	4.5
20	0.15	0.186	0.214	0.228	A-5	A-4	A-3	0.9958	256.2	268.4	257.6	3.9
0	0.15	0.186	0.214	0.228	A-5	A-4	A-3	0.9957	256.2	268.3	256.7	2.4

Table 9 Weight-minimization results of rotating three-layer tube in Case B-II

ω (rad/s)	A (m)	R_1 (m)	R_2 (m)	B (m)	Layer$_1$	Layer$_2$	Layer$_3$	$\Phi_{(c)}$	Best weight (kg/m)	Worst weight	Mean weight	Standard deviation
200	0.15	0.188	0.224	0.232	A-5	A-4	A-3	0.9988	272.7	280.5	273.3	1.5
180	0.15	0.206	0.208	0.228	A-5	S-5	A-4	0.9975	271.2	295.5	273.4	4.6
160	0.15	0.188	0.218	0.232	A-5	A-4	A-3	0.9986	272.2	296.4	274.4	6.5
140	0.15	0.188	0.216	0.232	A-5	A-4	A-3	0.9982	272.0	273.3	272.2	0.4
120	0.15	0.188	0.216	0.232	A-5	A-4	A-3	0.9965	272.0	298.5	275.9	8.8
100	0.15	0.188	0.216	0.23	A-5	A-4	A-4	0.9995	265.4	273.0	266.2	2.3
80	0.15	0.188	0.228	0.23	A-5	A-4	A-3	0.9998	265.2	295.2	266.5	6.0
60	0.15	0.188	0.228	0.23	A-5	A-4	A-3	0.9989	265.2	291.5	267.5	5.7
40	0.15	0.188	0.226	0.23	A-5	A-4	A-3	0.9997	265.0	295.2	267.0	6.2
20	0.15	0.188	0.226	0.23	A-5	A-4	A-3	0.9994	265.0	272.8	265.4	1.5
0	0.15	0.188	0.226	0.23	A-5	A-4	A-3	0.9992	265.0	265.4	265.1	0.2

Table 10 Cost-minimization results of BB-BC versus ADS in Case A-I ($T = 50$ °C)

Optimization algorithm	ADS			BB-BC		
	One-layer	Two-layer	Three-layer	One-layer	Two-layer	Three-layer
Best cost ($/m)	1421.4	1339.7	1312.0	1421.4	1339.7	1312.0
Worst cost	1421.4	1421.4	1385.9	1421.4	1339.7	1339.7
Mean cost	1421.4	1348.5	1344.8	1421.4	1339.7	1313.1
Standard deviation	0	21.5	24.3	0	0	5.5
Coefficient of variation (%)	0	1.6	1.8	0	0	0.4
Practical reliability (%)	100	96	84	100	100	100

Table 11 Cost-minimization results of BB-BC versus ADS in Case B-I ($\omega = 100$ rad/s)

Optimization algorithm	ADS			BB-BC		
	One-layer	Two-layer	Three-layer	One-layer	Two-layer	Three-layer
Best cost ($/m)	1421.4	1336.2	1307.5	1421.4	1336.2	1307.5
Worst cost	1421.4	1360.1	1373.1	1421.4	1336.2	1360.1
Mean cost	1421.4	1341.0	1338.0	1421.4	1336.2	1314.2
Standard deviation	0	9.8	20.9	0	0	14.3
Coefficient of variation (%)	0	0.7	1.6	0	0	1.1
Practical reliability (%)	100	100	96	100	100	100

Table 12 Weight-minimization results of BB-BC versus ADS in Case A-I ($T = 50$ °C)

Optimization algorithm	ADS			BB-BC		
	One-layer	Two-layer	Three-layer	One-layer	Two-layer	Three-layer
Best cost (kg/m)	258.4	257.3	256.3	258.4	257.3	256.3
Worst cost	258.4	258.4	281.3	258.4	257.3	272.6
Mean cost	258.4	257.5	260.7	258.4	257.3	259.1
Standard deviation	0	0.4	6.9	0	0	5.4
Coefficient of variation (%)	0	0.1	2.7	0	0	2.1
Practical reliability (%)	100	100	84	100	100	92

Table 13 Weight-minimization results of BB-BC versus ADS in Case B-I ($\omega = 100$ rad/s)

Optimization algorithm	ADS			BB-BC		
	One-layer	Two-layer	Three-layer	One-layer	Two-layer	Three-layer
Best cost (kg/m)	258.4	256.9	256.2	258.4	256.9	256.2
Worst cost	258.4	258.4	304.2	258.4	268.9	268.7
Mean cost	258.4	257.2	261.0	258.4	257.4	257.2
Standard deviation	0	0.3	10.5	0	2.4	3.3
Coefficient of variation (%)	0	0.1	4.0	0	0.9	1.3
Practical reliability (%)	100	100	88	100	100	100

two-, and three-layer tubes. For each design case, a discrete optimization problem is tackled where the employed metaheuristic algorithm attempts to select the optimal material type from Table 1 and thickness of each layer from multiples of 0.002 m. For the optimization process, the maximum number of iterations is set to 500, and a population of 50 individuals is employed to search the solution space. In all the investigated instances, the inner radius of the assemblies is set to $a = 0.15$ m. It is also worthwhile to note that due to the stochastic nature of the algorithm, in each design optimization case, the algorithm is executed 25 times and the details of the achieved best solution as well as the statistical results of all runs are tabulated.

Cost optimization of rotating one-, two-, and three-layer tubes is studied under different internal temperature values in Cases A-I and A-II, and the minimum cost results are presented in Fig. 3a, b. The corresponding detailed cost optimization results for rotating three-layer tubes are also presented in Tables 2 and 3. It is worth mentioning that in these tables $\Phi_{(c)}$ denotes the most critical value of the non-dimensional yield variable over the tube layers.

For the sake of clarity, the comparison of results is first carried out between the primary cases, i.e., Cases A and B, and discussions related to the fixed- and free-end assumptions (Cases I and II) are provided afterward. Here, angular speed and internal pressure of the tubes are set to $\omega = 150$ rad/s and $P = 150$ MPa, respectively, and the effect of the inner temperature is examined. The cost optimization results obtained in Cases A-I and A-II reveal that, on the one hand, by increasing the inner temperature from 0 to 100 °C, the optimum cost of all the one-, two- and three-layer assemblies decreases. On the other hand, it is apparent from the figures that by increasing the inner temperature, the difference between the optimum results of one-, two-, and three-layer tubes diminishes. Thus, it can be inferred that in the foregoing two cases fabricating two- and three-layer tubes instead of one-layer tubes would be more profitable under lower inner temperatures. Nevertheless, it should be noted that the conclusions drawn here are valid only for the investigated set of materials as well as considered loading and boundary conditions. For instance, as can be seen from Fig. 3a, b that for $T = 100$ °C the results of rotating three-layer tube are same as one- and two-layer tubes. Tables 2 and 3 present the numerical results for the above-mentioned three-layer tube under $T = 100$ °C for which three layers of A-5 aluminum alloy are found to be the most cost-efficient solution (i.e., the same solution of the associated one-layer tube). Contrary

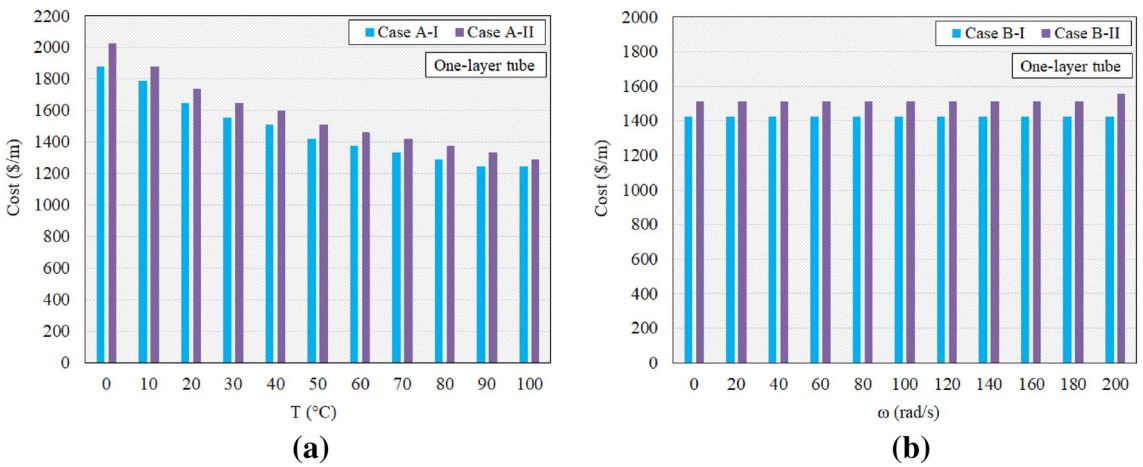

Fig. 5 Optimum cost for rotating one-layer tube: **a** Case A-I versus Case A-II; and **b** Case B-I versus Case B-II

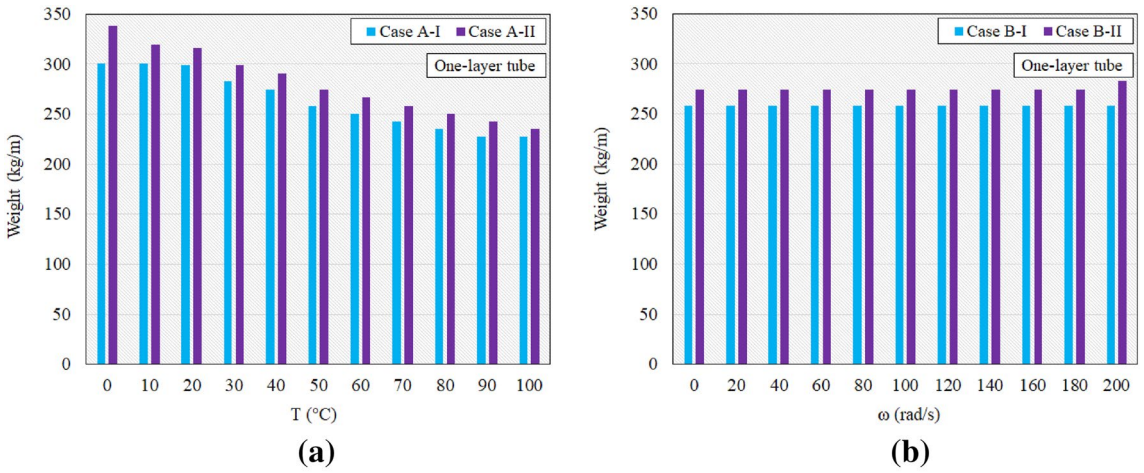

Fig. 6 Optimum weight for rotating one-layer tube: **a** Case A-I versus Case A-II; and **b** Case B-I versus Case B-II

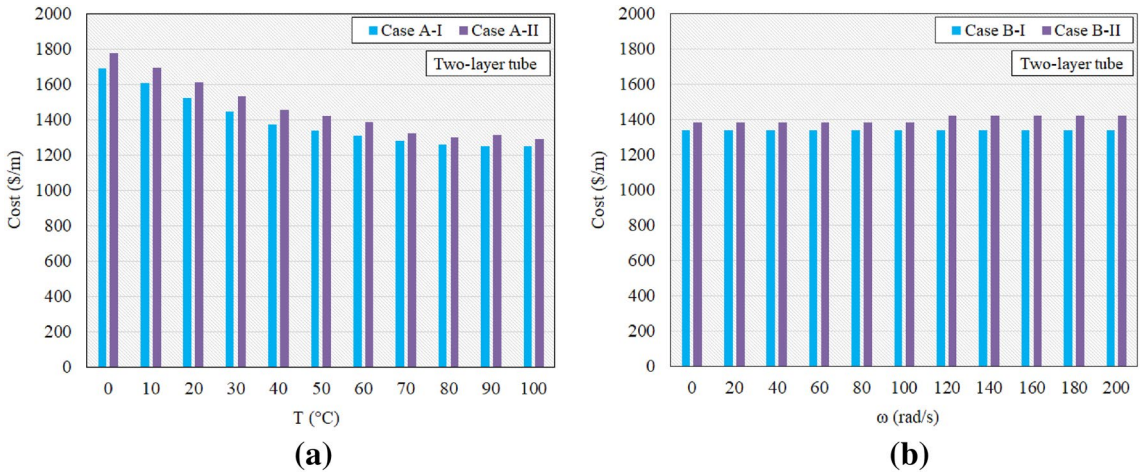

Fig. 7 Optimum cost for rotating two-layer tube: **a** Case A-I versus Case A-II and **b** Case B-I versus Case B-II

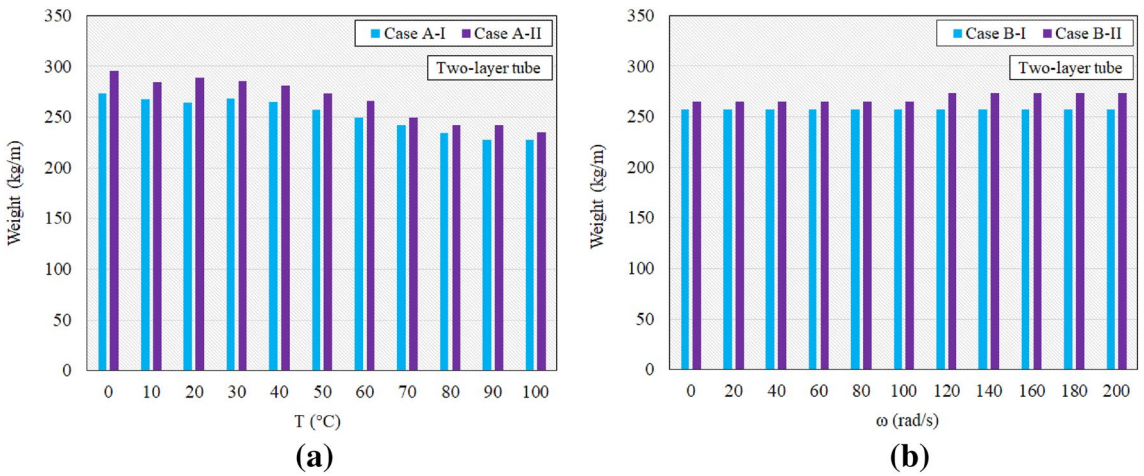

Fig. 8 Optimum weight for rotating two-layer tube: **a** Case A-I versus Case A-II and **b** Case B-I versus Case B-II

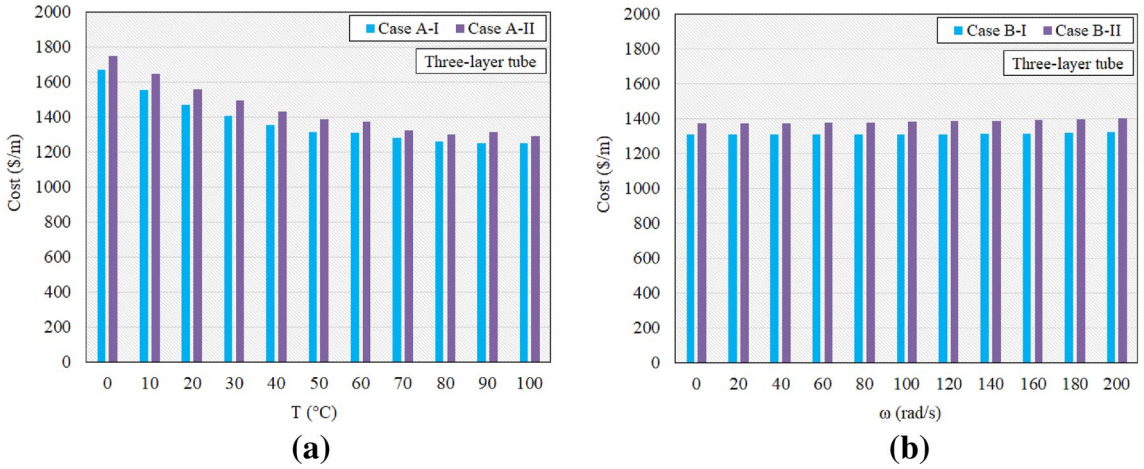

Fig. 9 Optimum cost for rotating three-layer tube: **a** Case A-I versus Case A-II and **b** Case B-I versus Case B-II

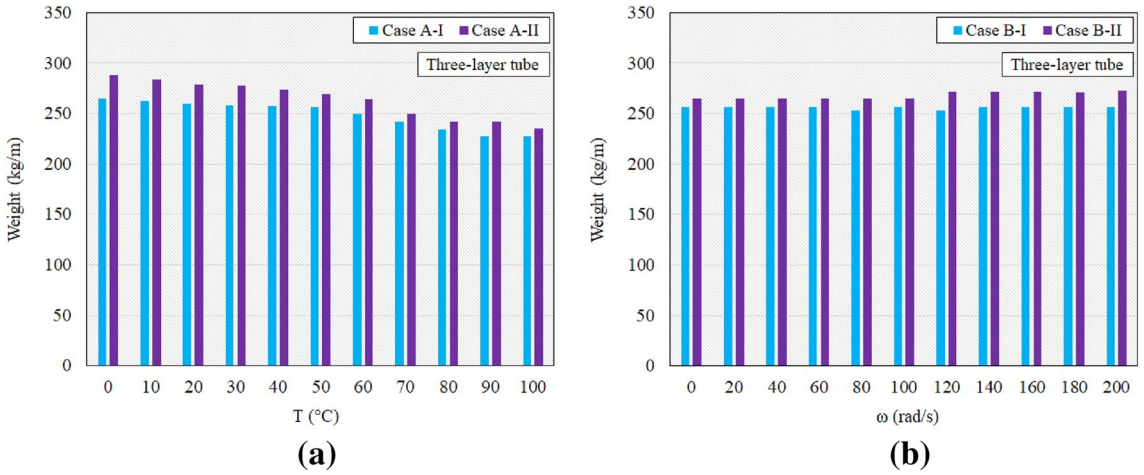

Fig. 10 Optimum weight for rotating three-layer tube: **a** Case A-I versus Case A-II and **b** Case B-I versus Case B-II

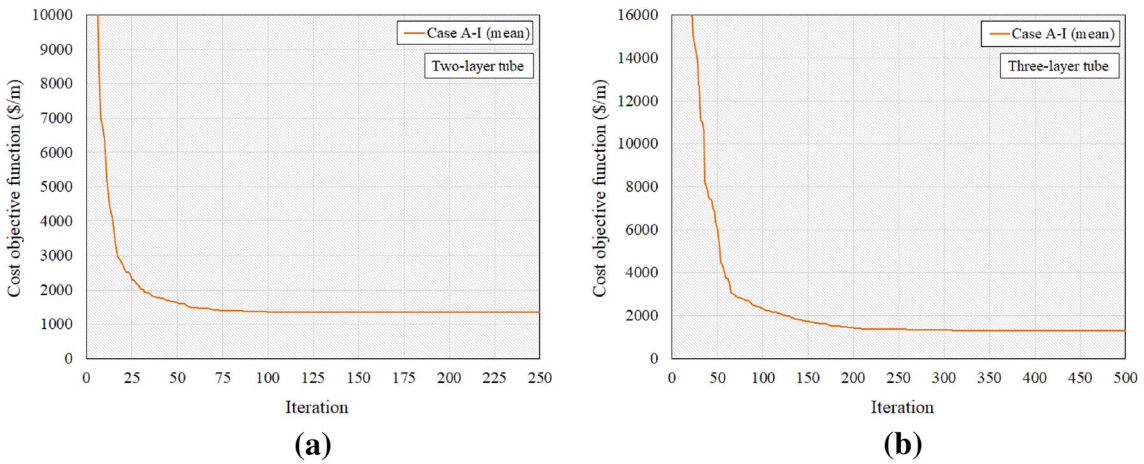

Fig. 11 Cost versus iterations plot of rotating **a** two-layer, and **b** three-layer tubes in Case A-I ($T = 50$ °C)

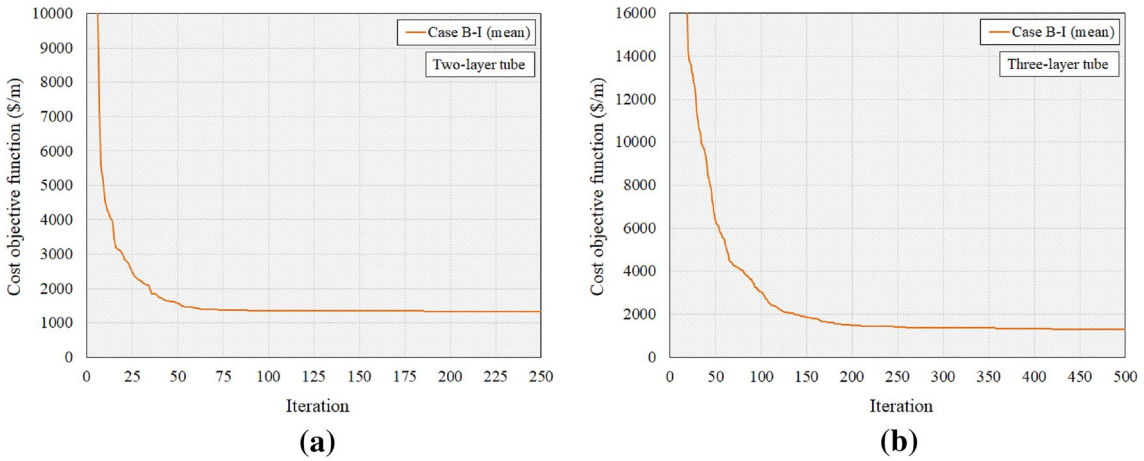

Fig. 12 Cost versus iterations plot of rotating **a** two-layer, and **b** three-layer tubes in Case B-I ($\omega = 100$ rad/s)

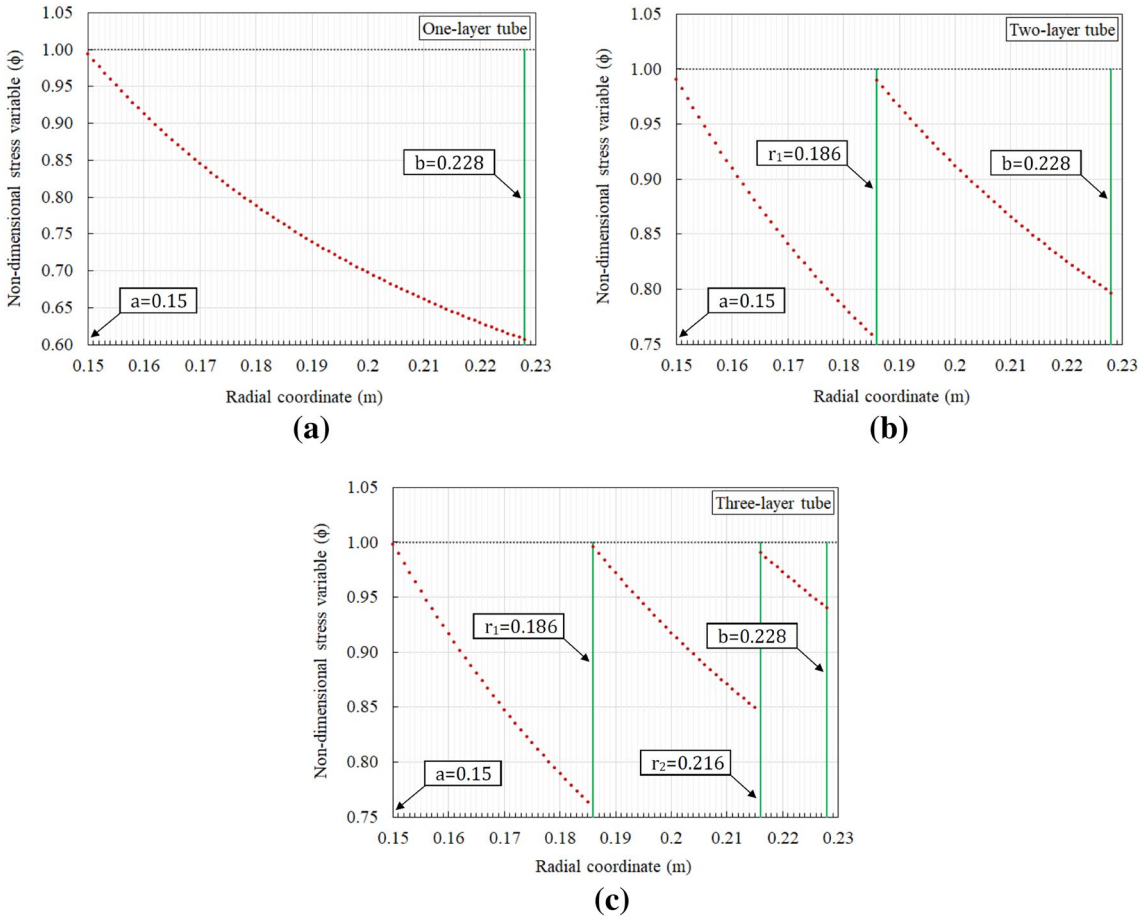

Fig. 13 Variations of non-dimensional stress variable in radial direction for minimum cost rotating **a** one-layer, **b** two-layer, and **c** three-layer tubes in Case A-I ($T = 50$ °C)

to the design found here using the set of steel and aluminum alloys given in Table 1, superior solutions for the same rotating three-layer tube could be achieved by increasing the size of material set, which entails further research.

Figure 3c, d depicts the minimum cost results of rotating one-, two-, and three-layer tubes in Cases B-I and B-II. The corresponding cost optimization results for rotating three-layer tubes are also tabulated in Tables 4 and 5. Here, internal temperature and pressure are set to $T = 50$ °C and P = 150 MPa, respectively, and the effect of angular speed of the assemblies is investigated. Although for different angular speeds, the two- and three-layer tubes produce more economical solutions compared to the one-layer designs, it can be deduced from the figures that increasing the angular speed of the assemblies from 0 to 200 rad/s results in relatively slight fluctuations in the optimum costs for all the investigated one-, two- and three-layer tubes. In Cases B-I and B-II, it is observed that the angular speed parameter does not play a governing role in the minimum cost design of the investigated assemblies.

Sometimes minimizing the total weight of an assembly could be the main objective of the optimization process. In this regard, Fig. 4a, b shows the weight optimization results for rotating one-, two-, and three-layer tubes in Cases A-I and A-II. The corresponding optimum designs for rotating three-layer tubes are given in Tables 6 and 7. As can be seen from Fig. 4a, b, by increasing the inner temperature from 0 to 100 °C, mostly—if not always—the optimum weight of all the one-, two- and three-layer assemblies decreases. Moreover, it is apparent from the figures that by increasing the inner temperature, the difference between the results of one-, two-, and three-layer tubes decreases. Hence, it can be deduced that in the above-mentioned two cases fabricating minimum weight two- and three-layer tubes instead of one-layer tubes would be more advantageous only for lower inner temperatures.

Weight minimization of rotating one-, two-, and three-layer tubes is also carried out in Cases B-I and B-II, and the results are shown in Fig. 4c, d. The obtained minimum weight solutions for rotating three-layer tubes are also presented in Tables 8 and 9. As already noted, in these cases, internal temperature and pressure are set to $T = 50$ °C and P = 150 MPa, respectively, and the effect of angular speed of the assemblies is examined. It can be seen from the figures that increasing the angular speed of the assemblies from 0 to 200 rad/s yields slight fluctuations in the optimum weights for all the studied one-, two-, and three-layer tubes. Similar to the cost optimization results, it is observed that in Cases B-I and B-II the angular speed parameter does not play a governing role in the minimum weight design of the investigated assemblies.

To further demonstrate the performance of the employed algorithm, Tables 10, 11, 12, and 13 show a comparison of the big bang-big crunch (BB-BC) algorithm versus the recently developed adaptive dimensional search (ADS) technique (Hasançebi and Kazemzadeh Azad 2015). The statistical results of 25 independent optimization runs presented in the above-mentioned tables show an acceptable level of comparability between the results of the BB-BC and ADS algorithms. Moreover, in order to quantify the consistency of the investigated optimization algorithms, the concept of practical reliability (Rama Mohan Rao et al. 2013) is used. The practical reliability indicates the ratio of successful solutions to the total number of independent executions of the optimization algorithm. In the present study, a successful solution is defined as a solution with a maximum difference of 5% from the best solution found by the algorithm over 25 independent runs.

As already mentioned, in this study, optimization of rotating one-, two-, and three-layer tubes is performed based on two different tube-end conditions (Cases I and II). For the sake of clarity, the cost and weight optimization results are separately compared for these two cases in Figs. 5, 6, 7, 8, 9, and 10. As can be seen from the figures, in all the investigated instances the obtained results in Case I (fixed-end assumption) are lighter/profitable than those achieved in Case II (free-end assumption). The presented results quantify and highlight the effect of assumptions made for structural response computations on the final designs. Average optimization histories of 25 independent runs are plotted in Figs. 11 and 12. It is worth mentioning that Figs. 11a and 12a are depicted up to 250 iterations since there is no significant improvement in the remaining iterations. Figure 13 shows the variations of non-dimensional stress variable φ in radial direction for typical rotating one-layer, two-layer, and three-layer tubes. As can be seen from the figure, the final designs satisfy the stipulated design constraint based on the von Mises yield criterion. The presented numerical results could provide some general guidelines for practical applications, especially in the preliminary design stage of rotating multilayer composite assemblies. Yet, it is noteworthy that although the present study is limited to optimization of rotating multilayer composite tubes under internal heating and pressure, the employed methodology can be further extended to handle optimization problems of rotating solid and annular disks as well. There is also scope for further research to include other set of materials as well as different loading and boundary conditions in the optimization process.

6 Conclusions

In the present work, both weight and cost minimization problems of rotating multilayer composite tubes are studied under internal heating and pressure. In order to determine the structural responses, analytical solutions are presented based on two different boundary conditions. The automated material selection and thickness optimization of pressurized one-, two-, and three-layer assemblies are performed under different angular speed and internal heating conditions using a contemporary metaheuristic optimization algorithm. The corresponding optimum solution for each angular speed as well as internal heating condition is sought, and the obtained designs are discussed. In Case A, where the effect of the inner temperature is examined, it is shown that by increasing the inner temperature from 0 to 100 °C, the difference between the results of one-, two-, and three-layer tubes decreases. Thus, it can be deduced that, in this case, fabricating minimum weight/cost two- and three-layer tubes instead of one-layer tubes would be more advantageous only for lower inner temperatures. Furthermore, in Case B, where the effect of angular speed of the assemblies is investigated, it is observed that increasing the angular speed of the assemblies from 0 to 200 rad/s yields slight fluctuations in the optimum weight/cost for all the investigated one-, two- and three-layer tubes. Moreover, considering the two different tube-end conditions, it is noticed that the obtained results in Case I (fixed-end assumption) are lighter/profitable than those achieved in Case II (free-end assumption) for all the test cases. The results quantify and highlight the effect of assumptions made for structural response computations on the optimality of final solutions. The foregoing results provide general guidelines for preliminary/conceptual design of rotating multilayer composite tubes under internal heating and pressure.

Compliance with Ethical Standards

Conflict of interest The authors declare that there is no conflict of interests regarding the publication of this paper.

References

Akbulut M, Sarac A, Ertas AH (2020) An investigation of non-linear optimization methods on composite structures under vibration and buckling loads. Adv Comput Des 5(3):209–231

Akis T, Eraslan AN (2005) Yielding of long concentric tubes under radial pressure based on von Mises criterion. J Fac Eng Arch Gazi Univ 20:365–372 **(In Turkish)**

Alkayem NF, Cao M, Zhang Y, Bayat M, Su Z (2018) Structural damage detection using finite element model updating with evolutionary algorithms: a survey. Neural Comput Appl 30:389–411

Apatay T, Mack W (2015) On the optimum design of rotating two-layered composite tubes subject to internal heating or pressure. Forsch Ing 79:109–122

Colorni A, Dorigo M, Maniezzo V (1991) Distributed optimization by ant colony. In: Proceedings of the first European conference on artificial life, USA, pp 134–142

Eraslan AN, Akis T (2005) Yielding of two-layer shrink-fitted composite tubes subject to radial pressure. Forsch Ing 69:187–196

Eraslan AN, Sener E, Argeso H (2003) Stress distributions in energy generating two-layer tubes subjected to free and radially constrained boundary conditions. Int J Mech Sci 45:469–496

Erbatur F, Al-Hussainy MM (1992) Optimum design of frames. Comput Struct 45:887–891

Erol OK, Eksin I (2006) A new optimization method: big bang-big crunch. Adv Eng Softw 37:106–111

Gen M, Zhang W, Lin L, Yun YS (2017) Recent advances in hybrid evolutionary algorithms for multi-objective manufacturing scheduling. Comput Ind Eng 112:616–633

Goldberg DE, Samtani MP (1986) Engineering optimization via genetic algorithm. In: Proceeding of the ninth conference on electronic computation. ASCE, pp 471–82

Hasançebi O, Kazemzadeh Azad S (2015) Adaptive dimensional search: a new metaheuristic algorithm for discrete truss sizing optimization. Comput Struct 154:1–16

Jahed H, Farshi B, Karimi M (2006) Optimum autofrettage and shrink-fit combination in multi-layer cylinders. Trans ASME J Press Vessel Technol 128:196–200

Kazemzadeh Azad S (2019) Monitored convergence curve: a new framework for metaheuristic structural optimization algorithms. Struct Multidiscip Optim 60(2):481–499

Kazemzadeh Azad S, Akış T (2018) Automated selection of optimal material for pressurized multi-layer composite tubes based on an evolutionary approach. Neural Comput Appl 29:405–416

Kazemzadeh Azad S, Akış T (2019) A study of shrink-fitting for optimal design of multi-layer composite tubes subjected to internal and external pressure. IJST Trans Mech Eng 43:451–467

Kennedy J, Eberhart R (1995) Particle swarm optimization. In: IEEE international conference on neural networks. IEEE Press, pp 1942–1948

Koç Ç (2017) An evolutionary algorithm for supply chain network design with assembly line balancing. Neural Comput Appl 28:3183–3195

Lee KS, Geem ZW (2004) A new structural optimization method based on the harmony search algorithm. Comput Struct 82:781–798

Lee ZY, Chen CK, Hung CI (2001) Transient thermal stress analysis of multilayered hollow cylinder. Acta Mech 151:75–88

MATLAB (2019) version 9.7 (R2019b) The MathWorks Inc., Natick, Massachusetts

Miraje AA, Patil SA (2012) Optimum thickness of three-layer shrink fitted compound cylinder for uniform stress distribution. Int J Adv Eng Technol 3(2):591–605

Noda N, Hetnarski RB, Tanigawa Y (2003) Thermal stresses, 2nd edn. Taylor and Francis, New York

Ootao Y, Tanigawa Y, Fukuda T (1991) Axisymmetric transient thermal stress analysis of a multilayered composite hollow cylinder. J Therm Stress 14:201–213

Rama Mohan Rao A, Lakshmi K, Ganesan K (2013) Structural system identification using quantum behaved particle swarm optimisation algorithm. SDHM Struct Durab Health Monit 9(2):99–128

Saka MP (1991) Optimum design of steel frames with stability constraints. Comput Struct 41:1365–1377

Sharifi M, Arghavani J, Hematiyan MR (2012) An analytical solution for optimum design of shrink-fit multi-layer compound cylinders. Int J Appl Mech 4:1250043

Sharifi M, Arghavani J, Hematiyan MR (2014) Optimum arrangement of layers in multi-layer compound cylinders. Int J Appl Mech 6:1450057

Tabak EI, Wright PM (1981) Optimality criteria method for building frames. J Struct Div ASCE 107:1327–1342

Timoshenko SP, Goodier JN (1970) Theory of elasticity, 3rd edn. McGraw-Hill, New York

Tutuncu N (1995) Radial stresses in composite thick-walled shafts. J Appl Mech 62:547–549

Tzeng JT (2002) Viscoelastic analysis of composite cylinders subjected to rotation. J Compos Mater 36:229–239

Zhou SS, Gao XL, Griffith GW (2012) Stress analysis and structural optimization of a three-layer composite cladding tube under thermo-mechanical loads. J Eng Mater Technol ASME 134(3):031001